Observation of variations in cosmic ray single count rates during thunderstorms and implications for large-scale electric field changes

R. U. Abbasi[1,*] T. Abu-Zayyad,[1,2] M. Allen,[2] Y. Arai,[3] R. Arimura,[3] E. Barcikowski,[2] J. W. Belz,[2] D. R. Bergman,[2] S. A. Blake,[2] I. Buckland,[2] R. Cady,[2] B. G. Cheon,[4] J. Chiba,[5] M. Chikawa,[6] T. Fujii,[7] K. Fujisue,[6] K. Fujita,[3] R. Fujiwara,[3] M. Fukushima,[6] R. Fukushima,[3] G. Furlich,[2] N. Globus,[8,†] R. Gonzalez,[2] W. Hanlon,[2] M. Hayashi,[9] N. Hayashida,[10] K. Hibino,[10] R. Higuchi,[6] K. Honda,[11] N. Husseini,[12] D. Ikeda,[10] T. Inadomi,[13] N. Inoue,[14] T. Ishii,[11] H. Ito,[8] D. Ivanov,[2] H. Iwakura,[13] A. Iwasaki,[3] H. M. Jeong,[15] S. Jeong,[15] H. Johnson,[1] C. C. H. Jui,[2] K. Kadota,[16] F. Kakimoto,[10] O. Kalashev,[17] K. Kasahara,[18] S. Kasami,[19] H. Kawai,[20] S. Kawakami,[3] S. Kawana,[14] K. Kawata,[6] I. Kharuk,[17] E. Kido,[8] H. B. Kim,[4] J. H. Kim,[2] J. H. Kim,[2] M. H. Kim,[15] S. W. Kim,[15] Y. Kimura,[3] S. Kishigami,[3] Y. Kubota,[13] S. Kurisu,[13] V. Kuzmin,[17,‡] M. Kuznetsov,[21,17] Y. J. Kwon,[22] K. H. Lee,[15] R. LeVon,[2] B. Lubsandorzhiev,[17] J. P. Lundquist,[23,2] K. Machida,[11] H. Matsumiya,[3] T. Matsuyama,[3] J. N. Matthews,[2] R. Mayta,[3] J. Mazich,[1] M. Minamino,[3] K. Mukai,[11] I. Myers,[2] P. Myers,[1] S. Nagataki,[8] K. Nakai,[3] R. Nakamura,[13] T. Nakamura,[24] T. Nakamura,[13] Y. Nakamura,[13] A. Nakazawa,[13] E. Nishio,[19] T. Nonaka,[6] K. O'Brien,[1] H. Oda,[3] S. Ogio,[25,3] M. Ohnishi,[6] H. Ohoka,[6] Y. Oku,[19] T. Okuda,[26] Y. Omura,[3] M. Ono,[8] R. Onogi,[3] A. Oshima,[27] S. Ozawa,[28] I. H. Park,[15] M. Potts,[2] M. S. Pshirkov,[17,29] J. Remington,[2] D. C. Rodriguez,[2] G. I. Rubtsov,[17] D. Ryu,[30] H. Sagawa,[6] R. Sahara,[3] Y. Saito,[13] N. Sakaki,[6] T. Sako,[6] N. Sakurai,[3] K. Sano,[13] K. Sato,[3] T. Seki,[13] K. Sekino,[6] P. D. Shah,[2] Y. Shibasaki,[13] F. Shibata,[11] N. Shibata,[19] T. Shibata,[6] H. Shimodaira,[6] B. K. Shin,[30] H. S. Shin,[6] D. Shinto,[19] J. D. Smith,[2] P. Sokolsky,[2] N. Sone,[13] B. T. Stokes,[2] T. A. Stroman,[2] Y. Takagi,[3] Y. Takahashi,[3] M. Takamura,[5] M. Takeda,[6] R. Takeishi,[6] A. Taketa,[31] M. Takita,[6] Y. Tameda,[19] H. Tanaka,[3] K. Tanaka,[32] M. Tanaka,[33] Y. Tanoue,[3] S. B. Thomas,[2] G. B. Thomson,[2] P. Tinyakov,[21,17] I. Tkachev,[17] H. Tokuno,[34] T. Tomida,[13] S. Troitsky,[17] R. Tsuda,[3] Y. Tsunesada,[25,3] Y. Uchihori,[35] S. Udo,[10] T. Uehama,[13] F. Urban,[36] T. Wong,[2] M. Yamamoto,[13] K. Yamazaki,[27] J. Yang,[37] K. Yashiro,[5] F. Yoshida,[19] Y. Yoshioka,[13] Y. Zhezher,[6,17] and Z. Zundel[2]

[1]*Department of Physics, Loyola University Chicago, Chicago, Illinois 60660, USA*
[2]*High Energy Astrophysics Institute and Department of Physics and Astronomy, University of Utah, Salt Lake City, Utah 84112, USA*
[3]*Graduate School of Science, Osaka City University, Osaka, Osaka 558-8585, Japan*
[4]*Department of Physics and The Research Institute of Natural Science, Hanyang University, Seongdong-gu, Seoul 04763, Korea*
[5]*Department of Physics, Tokyo University of Science, Noda, Chiba 278-8510, Japan*
[6]*Institute for Cosmic Ray Research, University of Tokyo, Kashiwa, Chiba 277-8582, Japan*
[7]*The Hakubi Center for Advanced Research and Graduate School of Science, Kyoto University, Kitashirakawa-Oiwakecho, Sakyo-ku, Kyoto 606-8224, Japan*
[8]*Astrophysical Big Bang Laboratory, RIKEN, Wako, Saitama 351-0198, Japan*
[9]*Information Engineering Graduate School of Science and Technology, Shinshu University, Nagano, Nagano 380-8553, Japan*
[10]*Faculty of Engineering, Kanagawa University, Yokohama, Kanagawa 221-8686, Japan*
[11]*Interdisciplinary Graduate School of Medicine and Engineering, University of Yamanashi, Kofu, Yamanashi 400-8510, Japan*
[12]*Illinois Mathematics and Science Academy, Aurora, Illinois 60506, USA*
[13]*Academic Assembly School of Science and Technology Institute of Engineering, Shinshu University, Nagano, Nagano 380-8553, Japan*
[14]*The Graduate School of Science and Engineering, Saitama University, Saitama, Saitama 338-8570, Japan*
[15]*Department of Physics, SungKyunKwan University, Jang-an-gu, Suwon 16419, Korea*
[16]*Department of Physics, Tokyo City University, Setagaya-ku, Tokyo 158-8557, Japan*
[17]*Institute for Nuclear Research of the Russian Academy of Sciences, Moscow 119991, Russia*
[18]*Faculty of Systems Engineering and Science, Shibaura Institute of Technology, Minato-ku, Tokyo 108-0023, Japan*
[19]*Department of Engineering Science, Faculty of Engineering, Osaka Electro-Communication University, Neyagawa-shi, Osaka 572-8530, Japan*
[20]*Department of Physics, Chiba University, Chiba, Chiba 263-8522, Japan*
[21]*Service de Physique Thorique, Universit Libre de Bruxelles, Brussels 1050, Belgium*
[22]*Department of Physics, Yonsei University, Seodaemun-gu, Seoul 03722, Korea*
[23]*Center for Astrophysics and Cosmology, University of Nova Gorica, Nova Gorica 5000, Slovenia*
[24]*Faculty of Science, Kochi University, Kochi, Kochi 780-8072, Japan*

^{25}*Nambu Yoichiro Institute of Theoretical and Experimental Physics, Osaka City University,*
Osaka, Osaka 558-8585, Japan
^{26}*Department of Physical Sciences, Ritsumeikan University, Kusatsu, Shiga 525-0058, Japan*
^{27}*College of Engineering, Chubu University, Kasugai, Aichi 487-8501, Japan*
^{28}*Quantum ICT Advanced Development Center, National Institute for Information and Communications*
Technology, Koganei, Tokyo 184-0015, Japan
^{29}*Sternberg Astronomical Institute, Moscow M.V. Lomonosov State University, Moscow 119991, Russia*
^{30}*Department of Physics, School of Natural Sciences, Ulsan National Institute of Science and Technology,*
UNIST-gil, Ulsan 44919, Korea
^{31}*Earthquake Research Institute, University of Tokyo, Bunkyo-ku, Tokyo 113-8654, Japan*
^{32}*Graduate School of Information Sciences, Hiroshima City University,*
Hiroshima, Hiroshima 731-3194, Japan
^{33}*Institute of Particle and Nuclear Studies, KEK, Tsukuba, Ibaraki 305-0801, Japan*
^{34}*Graduate School of Science and Engineering, Tokyo Institute of Technology,*
Meguro, Tokyo 152-8550, Japan
^{35}*Department of Research Planning and Promotion, Quantum Medical Science Directorate, National*
Institutes for Quantum and Radiological Science and Technology, Chiba, Chiba 263-8555, Japan
^{36}*CEICO, Institute of Physics, Czech Academy of Sciences, Prague 117 20, Czech Republic*
^{37}*Department of Physics and Institute for the Early Universe, Ewha Womans University,*
Seodaaemun-gu, Seoul 03760, Korea

We present the first observation by the Telescope Array Surface Detector (TASD) of the effect of thunderstorms on the development of cosmic ray single count rate intensity over a 700 km^2 area. Observations of variations in the secondary low-energy cosmic ray counting rate, using the TASD, allow us to study the electric field inside thunderstorms, on a large scale, as it progresses on top of the 700 km^2 detector, without dealing with the limitation of narrow exposure in time and space using balloons and aircraft detectors. In this work, variations in the cosmic ray intensity (single count rate) using the TASD, were studied and found to be on average at the $\sim(0.5\text{--}1)\%$ and up to 2% level. These observations were found to be both in excess and in deficit. They were also found to be correlated with lightning in addition to thunderstorms. These variations lasted for tens of minutes; their footprint on the ground ranged from 6 km to 24 km in diameter and moved in the same direction as the thunderstorm. With the use of simple electric field models inside the cloud and between cloud to ground, the observed variations in the cosmic ray single count rate were recreated using CORSIKA simulations. Depending on the electric field model used and the direction of the electric field in that model, the electric field magnitude that reproduces the observed low-energy cosmic ray single count rate variations was found to be approximately between 0.2 GV–0.4 GV. This in turn allows us to get a reasonable insight on the electric field and its effect on cosmic ray air showers inside thunderstorms.

I. INTRODUCTION

Understanding lightning initiation is one of the most important questions in atmospheric physics. The heart of the problem of understanding lightning initiation is that, with decades of electric fields measurements, the observed values of detected electric field are not sufficient to create a leader or a stroke propagating on a kilometer(s) scale [1,2]. This could mean that either our understanding of how lightning is initiated or electric field measurements in thunderstorms are inaccurate.

Traditionally, balloons and planes are used to make such measurements. However, there are limitations to obtaining such observations. At first, sending planes, balloons, and launching rockets inside thunderstorms can be quite difficult and dangerous. Moreover, thunderstorms can span up to square kilometers in size, while the electric field measured by airplanes and balloons spans a small region in comparison. To be in the right location at the right time where the electric field and the potential difference are of a high value can be of low probability. Most importantly, the instrument sent inside a thunderstorm might be responsible for discharging the thunderstorm itself before the electric field has the chance to build up.

When cosmic ray particles interact in the atmosphere, they produce a shower of secondary particles. During

---

*rabbasi@luc.edu
†Present address: University of Californa—Santa Cruz and Flatiron Institute, Simons Foundation.
‡Deceased

thunderstorms, these showers of secondary particles would accelerate or decelerate, depending on their charge and magnitude of the electric field they are propagating through. In principle, studying the effect of the electric field on these secondary particles would allow us to measure and model the electric field in their path indirectly.

The effect of thunderstorms on extensive air showers is a hot topic that has been reported on by multiple experiments starting with the Baksan Group in 1985 [3]. They argued that the effect of the observed cosmic ray variations in the hard and soft components of the shower are due to the electric field in the atmosphere. Several studies and observations have followed (EAS-TOP [4], Mount Norikura [5], GROWTH [6], Tibet AS [7], ARGO-YBJ [8], and SEVAN [9]) reporting on the cosmic ray secondary showers (electrons, gamma rays, muons, and neutrons) variation in correlation with thunderstorms. Most recently, a potential difference of greater than 1 GV inside a cloud (predicted by C. T. R. Wilson 90 years ago [10]) was indirectly measured in a storm by the GRAPES-3 Muon Telescope scientists [11]. Such potential difference is almost an order of magnitude larger than the previously reported maximum potential in balloon sounding (0.13 GV) [11,12].

In this work, we will present the effect of the electric field in thunderstorms on the extensive air showers as observed by the Telescope Array Surface Detector (TASD) single count rate. We will report on the observations in the variation of secondary cosmic-ray single-count rate (See the trigger level discussion in Sec. II). The variations are slow, several kilometers square in area, and move together with the thunderstorm on top of the 700 km^2 detector. In comparison to detectors that are spread over less than km^2 in area (i.e., [6]), it is unclear if the gamma ray emission ceases when the thunderstorm disappears, or when the gamma ray source moves away from the detectors observing the rate variation, as the thunderclouds move. We will attempt, to report on this question, for the first time, using a large area coverage of 700 km^2. Moreover, we will attempt to interpret this variation, by simulating the effect of the electric field in thunderstorms using multiple simple models. The corresponding increase and decrease of the rate variation in correlation with these models is reproduced and discussed.

II. THE TELESCOPE ARRAY DETECTOR

The Telescope Array (TA) detector is located in the southwestern desert of the State of Utah about 1400 m above sea level. Currently it is the largest Ultrahigh Energy Cosmic Ray (UHECR) experiment in the Northern Hemisphere. The TA detector is comprised of Surface Detectors (SDs) surrounded by three Fluorescence Detectors (FDs). The main goal of the TA detector is to explore the origin of UHECRs using their energy, composition, and arrival direction. The FD, which operates on

clear moonless nights (approximately 10% duty cycle) provides a measurement of the longitudinal profile of the Extensive Air Shower (EAS) induced by the primary UHECR, as well as a calorimetric estimate of the EAS energy. The SD part of the detector, with approximately 100% duty cycle, provides shower footprint information including core location, lateral density profile, and timing, which are used to reconstruct shower geometry and energy.

The surface detector utilizes plastic scintillators to observe the EAS footprint produced by primary cosmic ray interactions in the atmosphere. Plastic scintillators are sensitive to all charged particles. The surface detector array part of the TA experiment, is composed of 507 scintillator detectors on a 1.2 km square grid covering 700 km^2 in area shown in Fig. 1. Each surface detector houses two layers of plastic scintillator. Each layer of scintillator has an area of 3 m^2 and a thickness of 1.2 cm. Each plastic scintillator slab has grooves that has 104 WaveLength-Shifting (WLS) fibers running through them collecting light into the photomultiplier tubes (PMTs) they are bundled and connected to. These scintillator layers are separated by a 1 mm stainless-steel plate. The scintillator layers and stainless-steel plate are housed in light-tight, 1.5 mm thick box made of grounded stainless steel (the top cover is 1.5 mm thick, with a 1.2 mm thick bottom) under an additional 1.2 mm iron roof providing protection from extreme temperature variations [13].

There are a total of three trigger data levels—Level-0, Level-1, and Level-2. Charged particles triggering a single counter (both the upper and the lower scintillators) with an energy above approximately 0.3 Minimum Ionizing Particles (MIPs) ($\sim$0.75 MeV) are stored in a memory buffer on CPU board as Level-0 trigger data—the trigger rate is approximately 750 Hz. Charged particles triggering the detector with an energy above approximately 3 MIPs are stored as a Level-1 trigger event—the trigger rate is approximately 30 Hz. When three adjacent detectors trigger with an energy above 3 MIPs within 8 μs the data is saved as a Level-2 trigger—1 the trigger rate is approximately 0.01 Hz. The Level-2 trigger is the one used to study UHECRs and Level-0's main goal is to monitor the health of the detector. In this work we are using the rate of the detected particles every ten minutes recorded by the Level-0 trigger dominated by the single particles with primary energy ranging between $\sim$2 eV $\times 10^{10}$–10^{13} eV.

The TASD is designed to detect the charged components (primarily electrons, positrons, and muons) of the Extensive Air Shower (EAS). The response of the detector has been discussed in detail in [13,14]. Mostly muons and electrons are detected above approximately 30 MeV. Below this, the total energy deposited by muons and electrons falls off rapidly; below 1 MeV there is no detectable energy deposit as the electrons fail to penetrate a significant depth into the scintillator [14].
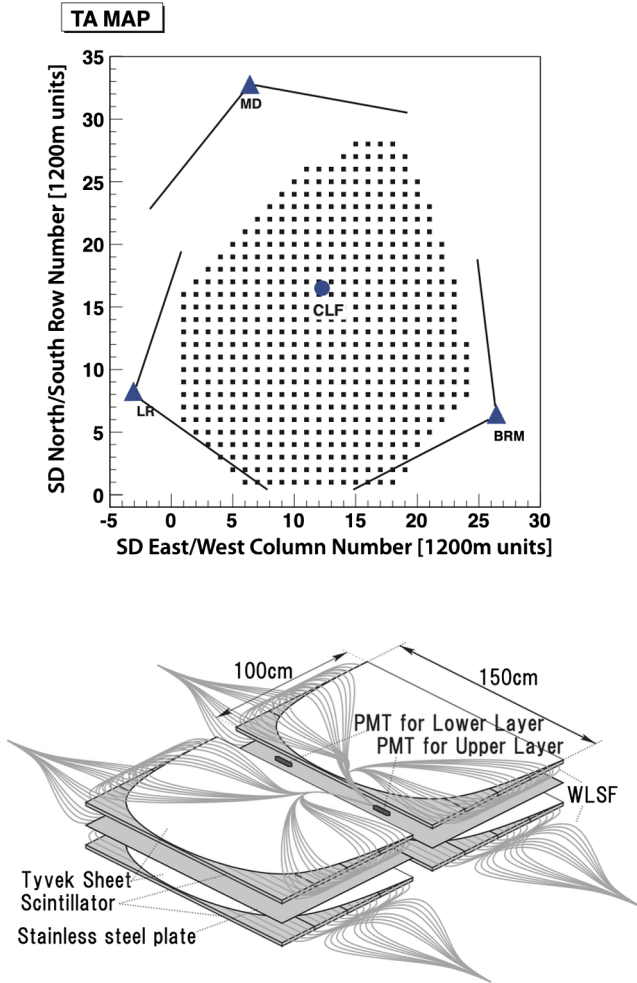
FIG. 1.   *Top:* The Telescope Array, consisting of 507 scintillator SDs on a 1.2 km grid over a 700 km^2 area. The SD scintillators are enclosed by three fluorescence detectors shown in filled triangles together with their field of view in solid lines. The northernmost fluorescence detector is called Middle Drum while the southern fluorescence detectors are referred to as Black Rock Mesa and Long Ridge. The filled circle in the middle equally spaced from the three fluorescence detectors is the central laser facility used for atmospheric monitoring and detector calibration. *Bottom:* Schematic sketch of the upper and lower 1.2 cm thick plastic scintillator layers inside the scintillator box, the 1 mm stainless steel plate, the 104 wavelength-shifting (WLS) fibers and the photomultiplier tubes. These items are enclosed in a stainless steel box, 1.5 mm thick on top and 1.2 mm thick on the bottom [13].

III. OBSERVATIONS

The Telescope Array detector has been in operation since 2008. Thunderstorms continuously pass on top of the Telescope Array detector. In this work, we searched for possible variation in the cosmic ray single count rate using Level-0 trigger in correlation with National Lightning Detection Network (NLDN) activity. There are typically about 750 NLDN recorded flashes (intracloud and cloud-to-ground) per year over the 700 km^2 TASD array. Due to

the large number of flashes only days with thunderstorms including a high recorded peak currents (>90 kA) are incorporated in the current search. For the Level-0 trigger data collected between 2008–2011, several thunderstorms were observed to produce a variation in the cosmic ray single count rate, the variations were observed during lightning events and in correlation with thunderstorms in the absence of lightning.

As an example, we chose an event observed on September 27, 2014 shown in Fig. 2. In Fig. 2, each frame lasts for ten minutes in duration. The time of the start of each frame is denoted on each frame in UTC. The color scale represents the change of the rate in Level-0 trigger of the current frame N_c from the ten-minute frame right before it N_p divided by N_p ($\frac{N_c - N_p}{N_p}$) or ($\Delta N/N$). Lightning events reported by the NLDN locations are also added in each of the frames in Figs. 2 and 6 in the Appendix. Intracloud in black and cloud-to-ground in gray. It is worth noting that three Terrestrial Gamma-Ray Flashes (TGFs) were reported in [14] on this day. One of these TGFs was reported at 07:54:35 (during the first frame in Fig. 2).

One can see a movement of a deficit in the intensity variation $\Delta N/N$ for 30 min (from 7:50–8:20 in UTC) in correlation with lightning activity. In addition, an excess was also found for 30 min (from 19:00–19:30 in UTC) in the intensity variation $\Delta N/N$ during which no lightning activity was reported by NLDN (Fig. 6 in the Appendix). These variations are both seen in correlation with lightning (using NLDN) and thunderstorms (using radar images as shown in Fig. 9 in the Appendix) in addition or in the absence of lightning [see Supplemental Material Videos (SM4, SM5) in [15]]. The variations correlation with pressure is not available at the current time resolution at the ground level. However, the variations were found to be not correlated with temperature changes at the ground level as shown in Figs. 3 and 7 in the Appendix. The size of the variation ranged for this thunderstorm from 6 km to 24 km in diameter on the ground. The variations were observed in excess and deficit modes over ten minutes in duration, mostly between $\pm(0.5–1)\%$ and can reach up to 2% in magnitude.

IV. CORSIKA SIMULATIONS

The main goal of this simulation work is to quantify the electric field inside thunderstorms resulting in the observed variations in the single count rate by the TASD detector. To do this we need to learn the conversion of the observed ($\Delta N/N$) into the equivalent potential model. This is done by inserting the atmospheric electric field model into the CORSIKA simulations. Here the CORSIKA package used in this simulation work is 7.6900 [17], where cosmic rays and their extensive air shower particles propagate through the atmosphere and through the implemented electric field
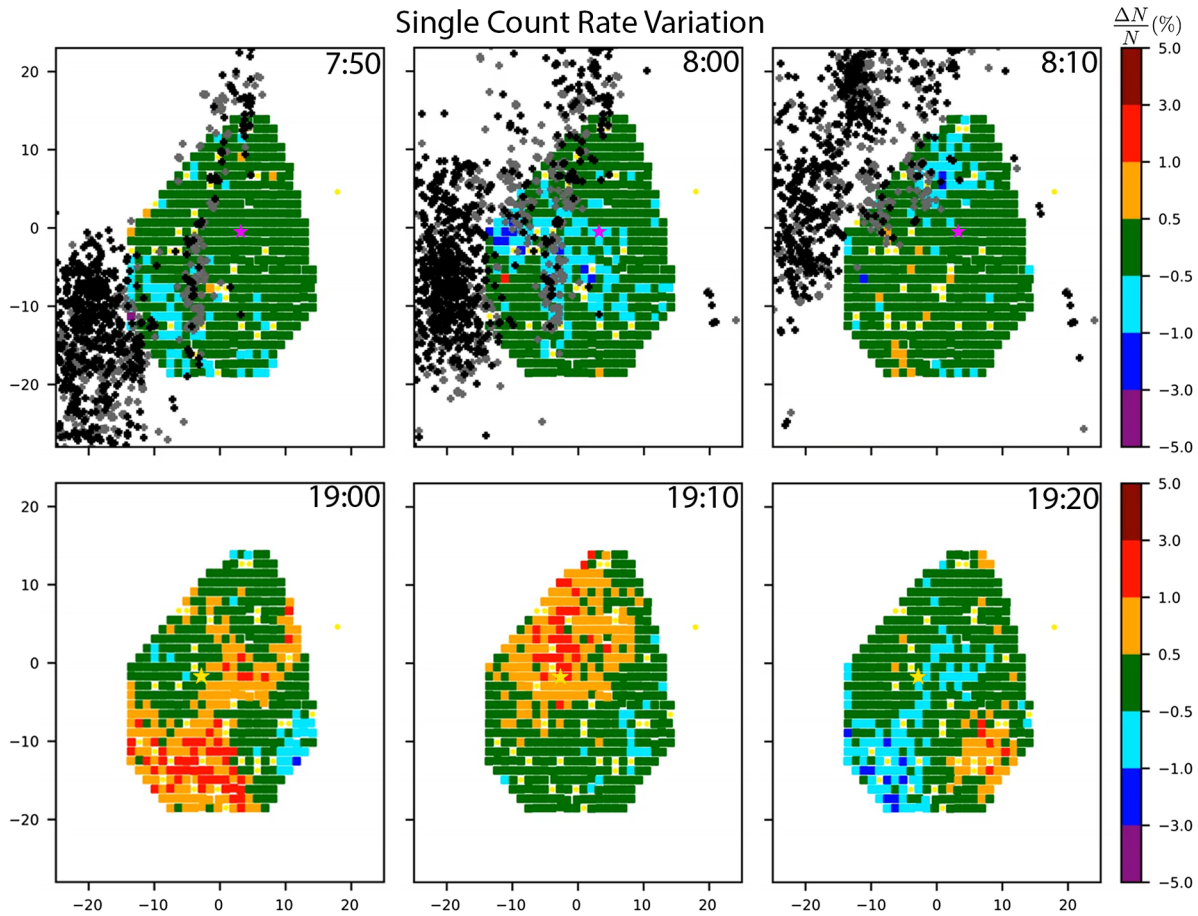
FIG. 2. Time evolution of the intensity variation of the single count rate change $(\frac{N_c - N_p}{N_p})\%$ or $(\Delta N/N)\%$ on the 09/27/2014 thunderstorm. Each time frame is ten minutes in duration. The starting time in UTC is denoted on each frame. The black and gray crosses marks are the intracloud and cloud-to-ground lightning sources detected by the NLDN for each frame. The two yellow and pink stars point at the two detectors [1516 (denoted in pink) and 1015 (denoted in yellow)] plotted in Fig. 3.

model. Both the electromagnetic and the muonic components of the showers are traced through the atmosphere and the implemented electric field model until they reach the detector observational level (~1400 m).

As a start, two electric field models are used. Note that both models chosen are the simplest electric field models that allow us to reproduce the main observed $(\Delta N/N)$ values. Both models use a uniform electric field layer. The first model uses a uniform electric field 2 km inside the thundercloud that is located 2 km above ground level. The second model uses a uniform electric field between the thundercloud base and the ground. Both models are illustrated in the Appendix (Fig. 8). In this second model the thundercloud base is 2 km in height from the detector. While thunderstorm structures are known to be complex, both the thundercloud length and height from the ground used in this work are reasonably representative of thunderstorms at the Southwestern desert of Utah [14].

Primary cosmic ray particles composed of protons were generated between 20 GeV–10 TeV. SIBYLL2.3c [18] is used for the high-energy interaction (>80 GeV). While, GHEISHA [19], URQMD [20], and FLUKA [21]
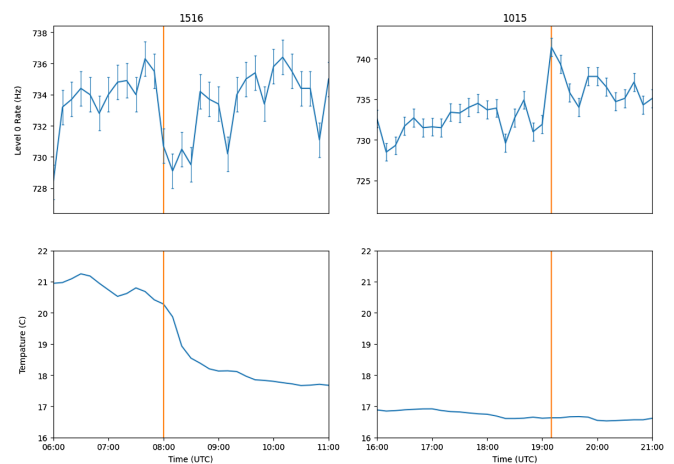
FIG. 3. Rate variation vs time and temperature variation vs time for two detectors numbered (1516 and 1015). Here 1516 shows a deficit in the rate variation (−0.8%) and 1015 shows an excess in the rate variation (+1.3%).
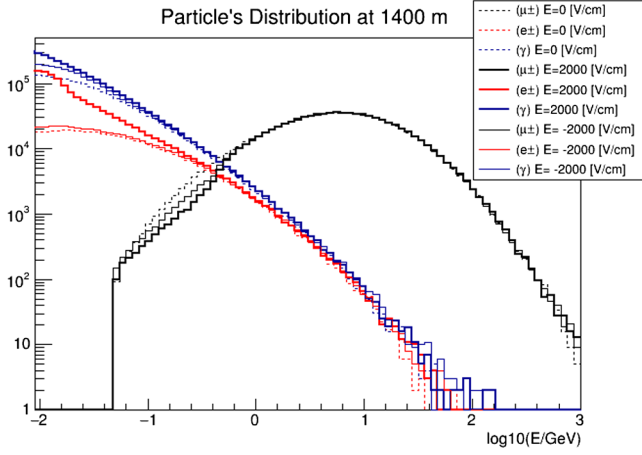
FIG. 4. The energy distributions of the muons and electromagnetic components of the EAS at 1400 m. The distribution of particles ($e^{\pm}, \mu^{\pm}, \gamma$) included in this plot are without electric field shown in dashed lines for the cloud-to-ground model and with electric field of $+2000$ V/cm (200 kV/m or 0.4 GV/2 km) effect on ($e^{\pm}, \mu^{\pm}, \gamma$) shown in thick solid lines and—2000 V/cm effect on ($e^{\pm}, \mu^{\pm}, \gamma$) shown in thin solid lines. Detector response is not included in this distribution.

are used for the low-energy model (< 80 GeV). The zenith and azimuth range from $0° \leq \theta \leq 60°$ and $0° \leq \phi \leq 360°$. The energy threshold of secondary particles were traced until they reach the following energies; 0.05 GeV for hadrons, 0.5 GeV for muons, 0.001 GeV for electrons, and 0.001 GeV for gammas.

The simulation was curried out first with no electric field for background. Second, by applying an electric field value that ranges between -2000 and $+2000$ V/cm (-200 and $+200$ kV/m). Figure 4 shows the distribution of the electromagnetic ($\gamma, e^{\pm}$) and muonic shower components ($\mu^{\pm}$) on the ground at 1400 m propagated through the atmosphere with electric field at ± 2000 V/cm and without

an electric field from cloud to ground. The air shower particles ($\gamma, e^{\pm}$, and $\mu^{\pm}$) are then propagated through the SD detector using an energy dependent response function derived from GEANT4 simulation of the surface detector [14] and following the same trigger condition as the Level-0 trigger. The dependence of $(\Delta N/N)$ on the potential inside the thunderstorms is shown in Fig. 5 using both thunderstorm electric field models described in this section. Note that, the direction of the electric field follows CORSIKA's definition, where positive electric field direction is pointing upwards.

V. DISCUSSION

The simulation results shown in Fig. 5 presents $(\Delta N/N)$ vs the potential difference (ΔV) for both investigated electric field models. The first model included a uniform electric field inside a cloud (*IntraCloud model*: Fig. 8, Left) with 2 km in thickness and two kilometers in height from the ground. This model produced both the excess and deficit observed in the variation in the cosmic ray single count rate. While we are unable to distinguish the type of triggering particle from plastic scintillators, simulations show that the deficit observed by the TASD is dominated by muons. In a negative electric field, an average deficit using the low energy models (GHEISHA, URQMD, and FLUKA), is $0.75 \pm 0.28\%$ obtained at -0.2 GV. In a positive electric field, an average deficit of $1.3^{+1.17}_{-1.38}\%$ is obtained at $+0.2$ GV. As shown in Fig. 2 the deficit observed by the TASD is mostly between 0.5% and 1% and can go up to 2%. This observed deficit is reproduced around ± 0.2 GV, using this model.

As the potential difference increases above 0.3 GV so does the variation in the cosmic ray single count rate turns from deficit to excess. The excess in the variation of $\Delta N/N$ strongly depends on the polarity of the electric field inside the thunderstorm in addition to the magnitude of the
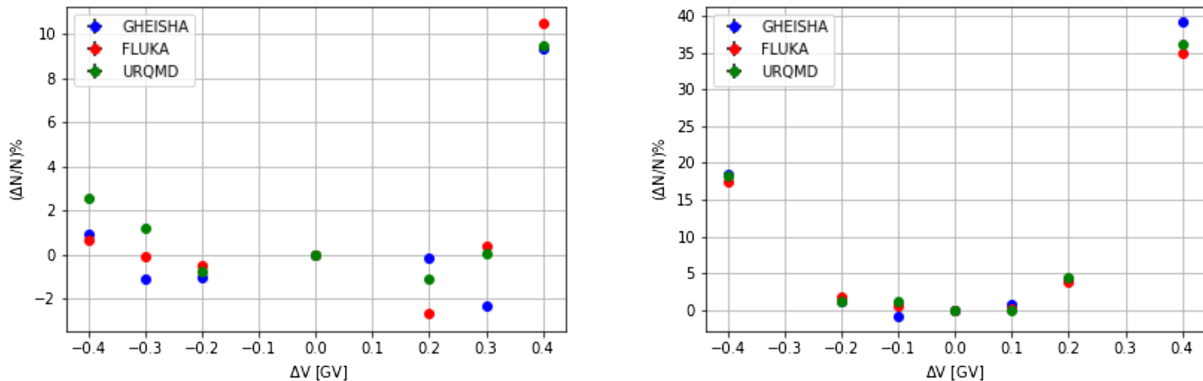

FIG. 5. Left: $(\Delta N/N)\%$ vs ΔV, including statistical error, for a uniform electric field layer inside the cloud (*IntraCloud model*) using the three low energy model GHEISHA, FLUKA, and URQMD. The model uses a uniform electric field 2 km inside the thundercloud that is located 2 km above ground level. Right: $(\Delta N/N)\%$ vs ΔV, including statistical error, for a uniform electric field layer between the cloud and ground (*Cloud-to-Ground model*) using the three low-energy model GHEISHA, FLUKA, and URQMD. In this model the thundercloud base is 2 km in height from the detector.

electric field. Simulations show that while the deficit in muons is stronger with a larger potential, an excess in the total number of particles observed by the TASD is expected as the variation of the soft components of the cosmic ray air shower dominates the total number of the observed particles. It also shows that the observed excess can be obtained depending on the low energy model and polarity. The TASD observed excess is mostly between 0.5% and 1% and can go up to 2%. In a negative electric field an average excess of $1.36^{+1.18}_{-0.44}\%$ is obtained at −0.4 GV. In the positive electric field, an average excess of 0.5%–2% is obtained with a potential between 0.3 GV and 0.4 GV. For the most part, the magnitude of ΔV needed to obtain the same observed variation is larger in the negative than in the positive electric field. This asymmetry is due to the fact that the number of electrons exceeds the number of positrons in the extensive air showers. This, in addition to the fact that, there are higher numbers of electrons with lower energies than positrons. Thus the effect of positive fields (accelerating electrons) is larger than the negative field (accelerating positrons) [8].

The second model included a uniform electric field of 2 km in length from the cloud to the ground (*Cloud-to-Ground model*: Fig. 8, right). This model produced only the excess in the variation in cosmic ray air single count rate (for the simulation sets produced). As in the first model, the excess in the total number of particles observed by the TASD is expected as the variation of the soft components of the cosmic ray air shower dominates the total number of observed particles. In a negative electric field, an average excess of $1.40^{+0.4}_{-0.2}\%$ can be produced by a potential difference of −0.2 GV. In a positive electric field, an excess of 0.5%—2% can be produced by a potential difference of less than 0.2 GV. The excess at a potential difference of −0.4 GV and 0.4 GV is 20% and 40% consecutively (much larger than the maximum observed excess of 2%). Therefore, we conclude that any observed excess resulting from this model is reproduced close to ±0.2 GV in potential.

It is important to note that, the interpretation of both models to the observations in the TASD single count variations is based on the assumption that the duration of the electric field inside the thunderstorm matches that of the duration of the ten minutes recorded observations by the Level-0 filter. However, the duration of the electric field could, in principle, be shorter than ten minutes and therefore we can assume that our current electric field interpretation is a lower limit value to the possible electric field magnitude that is responsible for the single rate observed variations.

VI. CONCLUSION

Variation in the flux of secondary low-energy cosmic ray counting rate in association with thunderstorms is reported in this work by the Telescope Array Surface Detector. The surface detector utilizes plastic scintillators to observe the charged components (primarily electrons, positrons, and muons) of the cosmic ray air shower. The variation in secondary low-energy cosmic-ray counting rate magnitude mostly ranges between (0.5% and 1%) and can reach up to 2%, both in excess and deficit, with a size that range from 6 km–24 km in diameter. This is the first observation of the variation in the secondary cosmic ray air showers covering 700 km^2 in size. Due to the large size of the TASD detector, we can clearly state that the intensity variations in the single count rates observed move in the same direction as the thunderstorms for tens of minutes at a speed of ∼20 km/10 min. These variations are both seen in correlation with lightning (using NLDN) and thunderstorms (using radar images) in the absence of lightning.

To interpret the effect of the electric field inside thunderstorms on the variation of the cosmic ray secondary shower flux, Monte Carlo simulations are performed with CORISKA. First, cosmic rays air showers are propagated in multiple electric field models, then the secondary shower particles (both soft and hard components of the shower) are propagated through the detector following the same trigger condition of the data used in this analysis. The total number of particles is then recorded and compared to simulation sets with no electric field. This simplified models used reproduced both the excess and deficit observed in the variation in the cosmic ray air shower flux. The electric field magnitude found to reproduce the observed intensity variations was approximately between 0.2 GV–0.4 GV, depending on the electric field model used and the direction of the electric field. Compared to previous observations, the potential difference recorded by TASD is larger than the reported maximum potential in balloon sounding (0.13 GV) [12]. However, the largest potential difference observed by a cosmic ray detector, thus far, was reported by the GRAPES-3 Muon Telescope, with a potential difference of 1 GV [11].

In order to interpret the observations of $\Delta N/N$ by the TASD, more precisely, it is clear that we need to know the polarity of the thunderstorm. This could in principle be achieved by implementing an array of Electric Field Mills (EFMs) at the Telescope Array site. This will allow us to better understand the polarity of the observed thunderstorms and therefore model them. Currently, an Electric Field Mill remote station has been installed approximately in the middle of the Telescope Array site for testing. This will enable us to study the relation between SD observations and the development of thunderstorm's electric field as it progresses on top of the Telescope Array detector.

ACKNOWLEDGMENTS

APPENDIX: SUPPORTING INFORMATION FIGURES

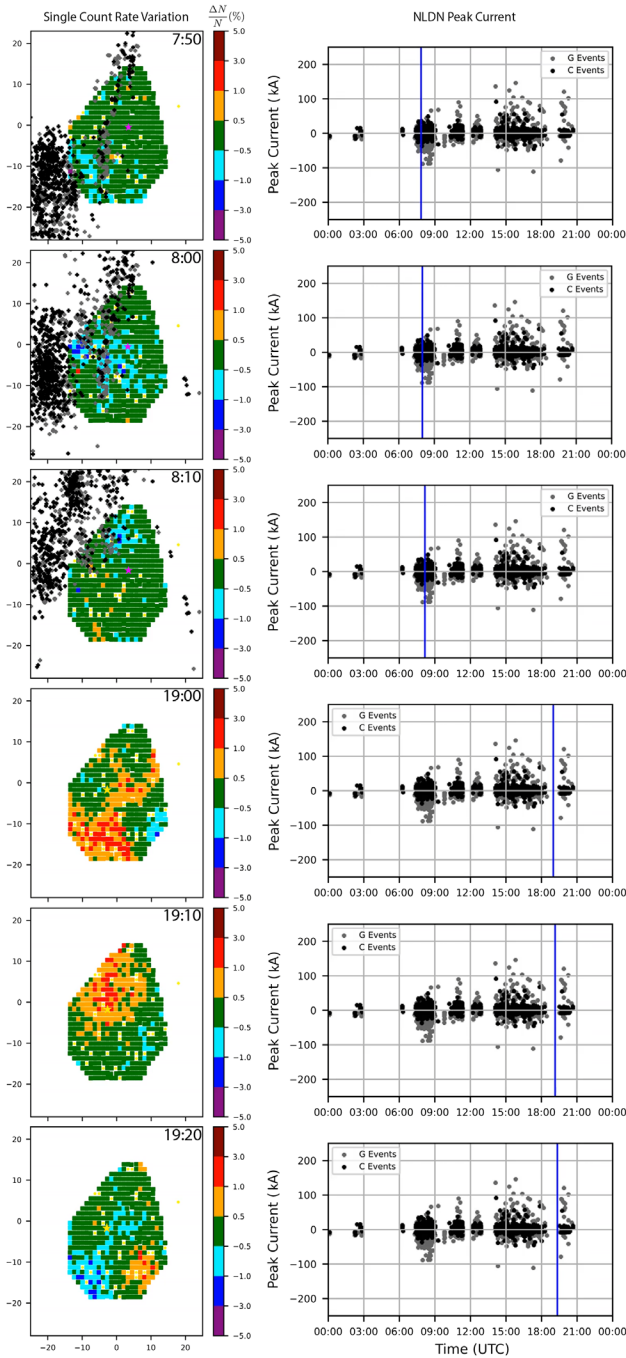In this appendix, we collect some figures that provide supporting information (Figs. 6–9).

FIG. 6. Left: Time evolution of the intensity variation of the secondary low-energy cosmic-ray counting rate change $(\frac{N_c - N_p}{N_p})$ or $(\Delta N/N)$ on the 09/27/2014 thunderstorm shown in Fig. 2. Right: NLDN events peak current (kA) vs. time of the day in UTC. The blue line denotes the starting time for each frame on the left hand side. The black and gray cross marks are the intracloud and cloud-to-ground lightning sources detected by the NLDN for each frame.
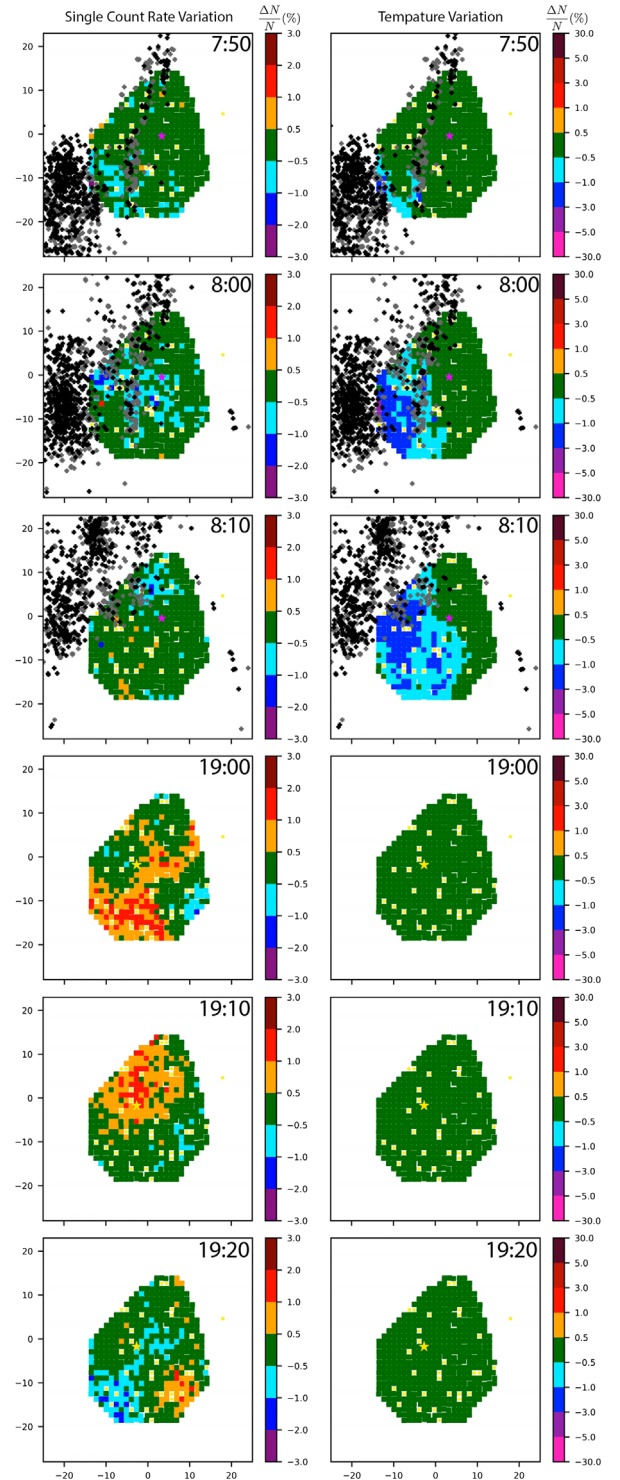
FIG. 7. Left: Time evolution of the intensity variation of the secondary low-energy cosmic-ray counting rate change $(\frac{N_c - N_p}{N_p})$ or $(\Delta N/N)$ on the 09/27/2014 thunderstorm shown in Fig. 2. Right: Temperature variation at 1400 m $(T_c - T_p)$ or (ΔT) for the same frames. T_c is the temperature in the current frame and T_p is the temperature in the previous frame. The starting time is denoted on each frame. The black and gray crosses marks are the intracloud and cloud-to-ground lightning sources detected by the NLDN for each frame.
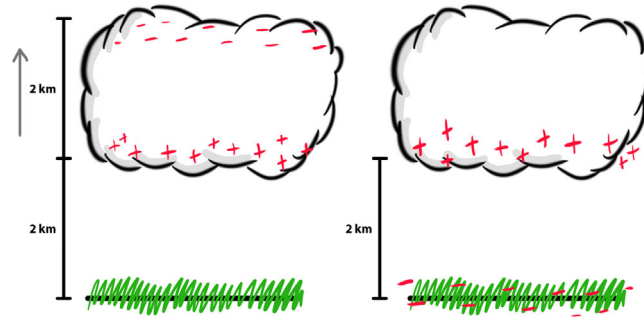
FIG. 8.   An illustration of the models used in the simulation in this work is to quantify the electric field inside thunderstorms resulting in the observed variations in the EAS by the TASD detector. left: The model using a uniform electric field 2 km inside the thundercloud (*Intra-Cloud model*) that is located 2 km above ground level. right: The model using a uniform electric field 2 km above ground level (*Cloud-to-Ground model*). The gray arrow represents the direction of the positive electric field following CORSIKA's definition, where positive electric field direction is pointing upwards.
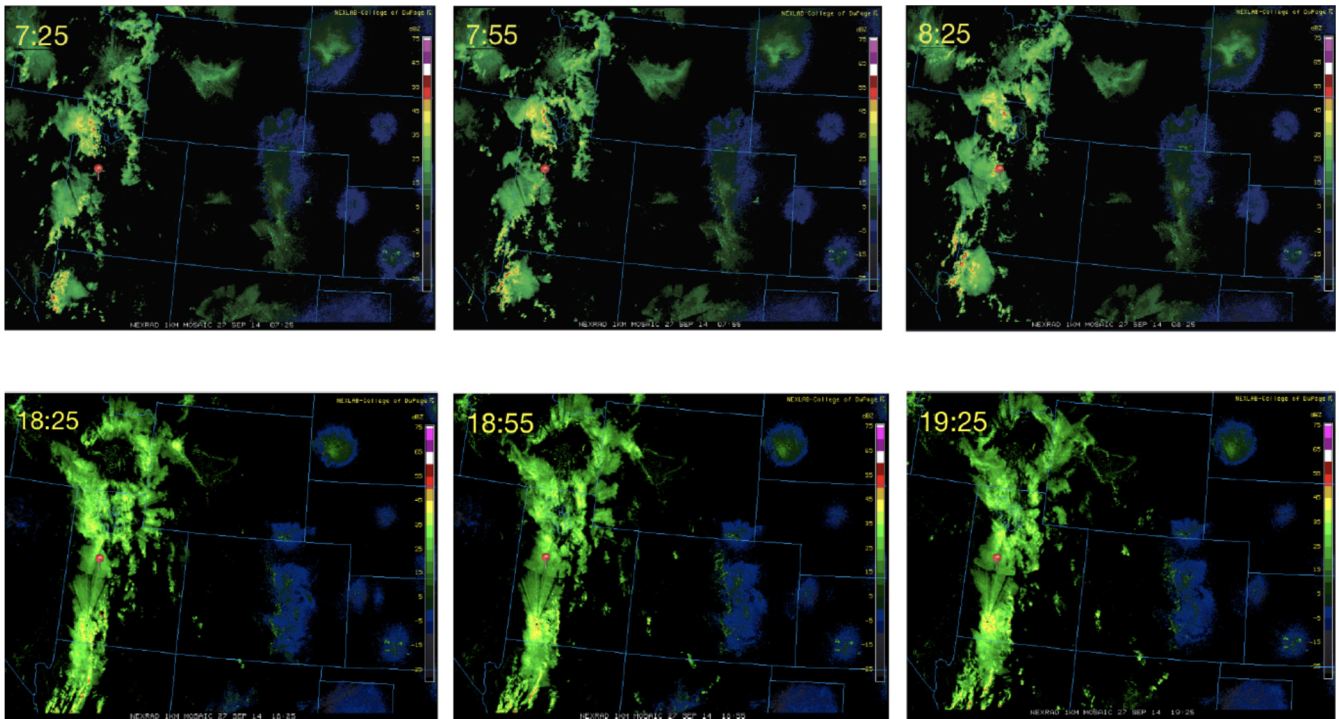

FIG. 9.   Top: Time evolution of the intensity variation of the radar images for the 09/27/2014 thunderstorm from 07:25–08:55 including the Telescope Array location marked in red. Bottom: Time evolution of the intensity variation of the radar images for the 09/27/2014 thunderstorm from 18:25–19:55 including the Telescope Array location marked in red.

[1] M. Stolzenburg, T. C. Marshall, W. David Rust, E. Bruning, D. R. MacGorman, and T. Hamlin, Electric field values observed near lightning flash initiations, Geophys. Res. Lett. **34** (2007).

[2] W. P. Winn, G. W. Schwede, and C. B. Moore, Measurements of electric fields in thunderclouds, J. Geophys. Res., **79**, 1761 (1974).

[3] V. V. Alexeenko *et al.*, Short perturbations of cosmic ray intensity and electric field in atmosphere, in *International Cosmic Ray Conference*, International Cosmic Ray Conference Vol. 4 (1987), p. 272.

[4] Eastop Collaboration, The EAS counting rate during thunderstorms, in *International Cosmic Ray Conference*, International Cosmic Ray Conference Vol. 10 (2001), p. 4165.

[5] Y. Muraki *et al.*, Effects of atmospheric electric fields on cosmic rays, Phys. Rev. D **69**, 123010 (2004).

[6] H. Tsuchiya *et al.*, Long-duration gamma ray emissions from 2007 and 2008 winter thunderstorms, J. Geophys. Res. **116** (2011).

[7] H. Tsuchiya *et al.*, Observation of thundercloud-related gamma rays and neutrons in Tibet, Phys. Rev. D **85**, 092006 (2012).

[8] B. Bartoli *et al.*, Observation of the thunderstorm-related ground cosmic ray flux variations by ARGO-YBJ, Phys. Rev. D **97**, 042001 (2018).

[9] K. Kudela *et al.*, Correlations between secondary cosmic ray rates and strong electric fields at lomnick tt, J. Geophys. Res. **122**, 10700 (2017).

[10] C. T. R. Wilson, Mathematical and physical sciences, Proc. R. Soc. A **236**, 297 (1956).

[11] B. Hariharan *et al.*, Measurement of the Electrical Properties of a Thundercloud through Muon Imaging by the GRAPES-3 Experiment, Phys. Rev. Lett. **122**, 105101 (2019).

[12] T. C. Marshall and M. Stolzenburg, Voltages inside and just above thunderstorms, J. Geophys. Res. **106**, 4757 (2001).

[13] T. Abu-Zayyad *et al.*, The surface detector array of the Telescope Array experiment, Nucl. Instrum. Methods Phys. Res., Sect. A **689**, 87 (2012).

[14] R. U. Abbasi *et al.*, Gamma ray showers observed at ground level in coincidence with downward lightning leaders, J. Geophys. Res. **123**, 6864 (2018).

[15] See Supplemental Material at http://link.aps.org/supplemental/10.1103/PhysRevD.105.062002 for time evolution of the radar images for the 09/27/2014 thunderstorm from 06:25 to 08:55 including the Telescope Array location marked in red (SM4) and for time evolution of the radar images for the 09/27/2014 thunderstorm from 18:25 to 19:50 including the Telescope Array location marked in red (SM5). These image were extracted from [16].

[16] https://www2.mmm.ucar.edu/imagearchive/image.

[17] D. Heck *et al.* Report No. FZKA 6019, vol. Forschungszentrum Karlsruhe, 1998.

[18] E.-J. Ahn, R. Engel, T. K. Gaisser, P. Lipari, and T. Stanev, Cosmic ray interaction event generator SIBYLL2.1, Phys. Rev. D **80**, 094003 (2009).

[19] H. Fesefeldt, Report No. PITHA-85/02, vol. RWTH Aachen, 1985.

[20] S. Bass *et al.*, Microscopic models for ultrarelativistic heavy ion collisions, Prog. Part. Nucl. Phys. **41**, 255 (1998).

[21] A. Fasso *et al.*, The Physics models of FLUKA: Status and recent developments, eConf, **C0303241**, MOMT005 (2003).